A superoxide dismutase mimic with high activity: crystal structure, solution equilibrium and pulse radiolysis

Jian-Jun Zhang,[ab] Qin-Hui Luo,*[ab] De-Liang Long,[b] Jiu-Tong Chen,[b] Feng-Mei Li[c] and An-Dong Liu[c]

[a] State Key Laboratory of Coordination Chemistry, Coordination Chemistry Institute,
   Nanjing University, Nanjing 210093, P. R. China. E-mail: qhluo@jlonline.com
[b] Fuzhou State Key Laboratory of Structure Chemistry, Fuzhou 350002, P. R. China
[c] Institute of Low Energy Nuclear Physics, Beijing Normal University, Beijing 100875,
   P. R. China

A new binuclear copper(II) complex [Cu$_2$(H$_{-4}$tapt)]·10H$_2$O, where tapt is N,N',N'',N'''-tetra(2-aminopropyl)-1,1,2,2-ethanetetraamide, has been synthesized and investigated in detail as a mimic of superoxide dismutase. Crystal structure analysis shows that each copper atom is situated in a slightly distorted square-pyramidal environment, with a water molecule at the apex. According to the result of pulse radiolysis, the complex has a high rate constant toward ˙O$_2^-$, k_{cat} = 1.91 × 10^8 dm^3 mol^{-1} s^{-1} (pH 7.4). Potentiometric titration shows that the mimic exhibits high stability at physiological pH value (7.4). EPR and ES-MS spectra reveal intermolecular interaction of two copper(II) nuclei.

Introduction

Superoxide dismutase (SOD) catalyses the dismutation of superoxide anion (˙O$_2^-$) and plays an important role in the protection of cells against oxygen toxicity.[1] Superoxide anion is the one-electron-reduction product of O$_2$ in mammalian organisms and the mediator of many diseases. It is involved in DNA damage, lipid peroxidation, radiation injury, and vascular diseases, *etc*.[2] In a variety of scenarios, therapeutic dosage of SOD enzyme has been promised,[3] but SOD has many shortcomings, such as short lifetime, high cost, tissue impermeability and immunogenicity, *etc*. Therefore the stable, non-toxic metal complexes (model compounds) which catalyse the dismutation of ˙O$_2^-$ offer considerable promise as SOD mimics for pharmaceutical application and have attracted much attention.[4] Although many SOD mimics have been reported, such as copper(II) complexes of polypeptides,[5] polydentate Schiff bases,[6] mixed ligands[7] and imidazolate-bridged heterobinuclear Cu–Zn complexes[8] or binuclear copper complexes,[9] complexes of macrocyclic ligands,[8b,10] and so on, only a few mimics which are both thermodynamically stable and highly active in the range of physiological pH were reported.[9,11] Therefore searching both highly stable and active complexes in aqueous solution as SOD mimics for pharmaceutical application has been a challenge for bioinorganic chemists.

Copper(II) ion is the active center of CuZnSOD. It is co-ordinated to four imidazole nitrogen atoms and one imidazole serves as a bridging ligand between Cu^{II} and Zn^{II}. In addition, a water molecule is co-ordinated to copper atom at the apex, forming a distorted square-pyramidal configuration.[12] The main function of Zn^{II} is to stabilize the protein structure and it has little effect on the activity of the enzyme. The structures of dioxotetraamine ligands are similar to those of polypeptides and they have the ability to stabilize high oxidation states of metal ions. The hydrogen of the amide group is lost upon co-ordination of divalent metal ions, and stable complexes may be formed.[13] Their transition metal complexes have been used as models of enzymes,[14] their macrocyclic copper(II) complexes have antiinflammatory activity,[15] and non-cyclic copper(II) complexes have therapeutic effect for rheumatoid arthritis.[16]

We have synthesized a linear double-cavity ligand N,N',N'', N'''-tetra(2-aminoethyl)-1,1,2,2-ethanetetraamide[11] (taet) whose structure is similar to that of bisdioxocyclam.[24] Its binuclear copper(II) complex [Cu$_2$(H$_{-4}$taet)] may effectively scavenge reactive oxygen species in organisms.[17] We modified its structure and obtained a new binuclear copper(II) complex [Cu$_2$(H$_{-4}$tapt)]·10H$_2$O (see Fig. 5), where tapt denotes N,N',N'',N'''-tetra(2-aminopropyl)-1,1,2,2-ethanetetraamide. The complex has a similar structure to that of the active site of CuZnSOD. pH Titration and pulse radiolysis were used to investigate its stability in aqueous solution and activity for superoxide anion dismutation. As four methyl groups were introduced in the backbone of the ligand, the new complex [Cu$_2$(H$_{-4}$tapt)]·10H$_2$O has better stability than that of [Cu$_2$(H$_{-4}$taet)] in aqueous solution, and also has high activity. In addition, its electrochemical behaviour, electrospray mass spectrum and the reaction mechanism for dismutation of superoxide anion have been investigated.

Experimental

Materials

Tetraethyl 1,1,2,2-ethanetetracarboxylate was synthesized according to the literature.[18] The reagents used for the solution studies were of reagent grade and the solutions prepared using twice-distilled water. Carbonate-free NaOH for pH titration was obtained by Powell's method.[19] A stock solution of Cu(NO$_3$)$_2$ approximately 1.0 × 10^{-2} mol dm^{-3} for pH titration was standardized by using Na$_2$edta. The content of HCl in the ligand was analysed by conductometric titration using a BSD-A conductometer. In pulse radiolysis experiments all the reagents were recrystallized twice in twice-distilled water. The solutions for pulse radiolysis contain about 3.21 × 10^{-6}–1.32 × 10^{-5} mol dm^{-3} Cu(ClO$_4$)$_2$ and tapt, molar ratio of Cu:tapt 2:1.4, and 0.1 mol dm^{-3} HCO$_2$Na, pH kept at 7.4 by using phosphate buffer.

Preparation of compounds

tapt and tapt·4HCl·EtOH·0.5H$_2$O. Tetraethyl 1,1,2,2-ethanetetracarboxylate (10 g, 0.03 mol) was added to a 1,2-diamino-

propane solution (100 cm³, 1.22 mol) at 0 °C. The resulting solution was stirred for one week, then the remaining 1,2-diaminopropane was distilled off under reduced pressure and the ligand isolated, washed with diethyl ether and dried in a vacuum desiccator. Yield 11.6 g (90%). The ligand tapt can be used for the subsequent synthesis without further purification. The very hygroscopic ligand was converted into the hydrochloride salt tapt·4HCl·EtOH·0.5H₂O for further studies. Thus tapt (2 g, 4.04 mmol) was dissolved in 10 cm³ methanol, then a dry stream of HCl was introduced. The resulting white precipitate was filtered off and recrystallized twice in MeOH–EtOH (1:1), then dried over P_2O_5 in vacuum desiccator. Yield 1.17 g (40%) (Found: C, 38.41; H, 7.47; N, 17.52; HCl, 22.85%. $C_{20}H_{49}Cl_4N_8O_{5.5}$ requires: C, 38.04; H, 7.82; N, 17.74; HCl, 23.09%). $\tilde{\nu}_{max}/cm^{-1}$(KBr) 3380m [$\nu$(N–H)] and 1665s [$\nu$(C=O)]. ^{1}H NMR (500 MHz, D₂O, 295 K): δ 3.63 (1 H, s, COCH₂CO), 3.58 (4 H, d, CONHCH₂), 3.51 (6 H, d, CH₃) and 3.43 (2 H, q, MeCHNH₂).

[Cu₂(H₋₄tapt)]·10H₂O. To an aqueous solution (50 cm³) of tapt (1 g, 2.32 mmol) was added 4.5 mmol of copper(II) hydroxide suspended in 500 cm³ water. The resulting solution was stirred at 50 °C for about 3 h, and filtered. The reddish violet crystals were isolated after concentration of the solution under reduced pressure. Yield 0.85 g (50%) (Found: C, 28.99; H, 7.26; N, 14.98; H₂O, 25.41%. $C_9H_{27}CuN_4O_7$ requires: C, 29.46; H, 7.42; N, 15.27; H₂O, 24.55%). $\tilde{\nu}_{max}/cm^{-1}$ (KBr) 3385m [ν(N–H)], 3700–2800s (hydrogen bonds) and 1600s [ν(C=O)]. λ_{max}/nm (water) 532 (ε/dm³ mol⁻¹ cm⁻¹ 16.4) and 260.2 (4744). Λ_m (water, 298 K) 8.3 S cm² mol⁻¹. μ/μ_B (295 K, per Cu) 2.05. Single crystals suitable for X-ray structure analysis were obtained by slow evaporation of the mother liquor for one week.

Pulse radiolysis

The apparatus consisted of a BF-5 linear electron accelerator and an optical monitor system. The electron pulse had an energy of 10 MeV, a beam current maximum of 150 mA and pulse width of 2.6 μs. The analytical light source was a 500 W xenon lamp powered by a voltage-current stabilizer. Dosimetry used ˙(SCN)₂ formed in N₂O-saturated 0.1 mol dm⁻³ KSCN solution, with ε = 7600 dm³ mol⁻¹ cm⁻¹ at 475 nm.[20] In this work the dose was measured to be 30 krad. The solutions of complex were placed in a Suprasil quartz cell (diameter 1 cm, length 1.4 cm). Before the electron beam entered into the reaction cell, superpure oxygen gas was bubbled into the solutions for 15 min. The optical density of ˙O₂⁻ was recorded immediately after one single electron pulse was injected into solutions. The molar absorption coefficient of ˙O₂⁻ at 250 nm is 2000 dm³ mol⁻¹ cm⁻¹. The ˙O₂⁻ concentration produced by one single electron pulse was calculated to be 7.2×10^{-5} mol dm⁻³.

pH Titration

Protonation constants of the ligand and stability constants of the copper(II) complexes were determined by using a Corning pH meter with a glass–silver–silver chloride combination electrode with precision ±0.001 pH. The electrode was standardized by buffer solutions of potassium hydrogenphthalate and sodium borate. Typical concentrations of the experimental solutions of ligand were 0.002755 mol dm⁻³, and the molar ratio of tapt·4HCl:Cu(NO₃)₂:HNO₃ was controlled to be 1:1:1 or 1:2:1. The experimental solutions were titrated with carbonate-free 0.09406 mol dm⁻³ NaOH by using a microsyringe with precision ±2 μl under a nitrogen atmosphere in a sealed jacketed vessel at 25 °C.[21] The ionic strength was kept at 0.10 mol dm⁻³ with KNO₃. For each system, at least two titrations have been performed, each of them having no less than 60 experimental points.

The equilibria in the system can be represented by eqn. (1)

$$qM + pH + rL \rightleftharpoons M_qH_pL_r \qquad (1)$$
$$\beta_{pqr} = [M_qH_pL_r]/[M]^q[H]^p[L]^r$$
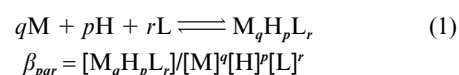
where q, p, and r denote the number of metal ions, hydrogen ions and ligand molecules bound in the complex respectively. A negative p value shows that hydrogen ion is released during co-ordination. The values of β_{pqr} were calculated by using the program LEMIT[21a] which is based on the Newton–Raphson and Gauss–Newton methods to minimize U in eqn. (2) where

$$U = \Sigma \, (C_{Hi}^{calc} - C_{Hi}^{expt})^2 \qquad (2)$$

C_{Hi}^{calc} and C_{Hi}^{expt} denote calculated and experimental values of the H⁺ concentration at the ith point respectively.

Electrochemical measurements

The experiments were carried out on a PAR Model 273 potentiostat coupled to a PAR Model 175 universal programmer. In CV measurements a glassy carbon electrode was employed as working electrode, a saturated calomel electrode (SCE) as reference electrode and platinum coil wire as auxiliary electrode. Experiments were performed under a purified nitrogen atmosphere at 25 ± 0.1 °C. The complex concentration was 1.0×10^{-3} mol dm⁻³ in 0.5 mol dm⁻³ sodium sulfate aqueous solution. The solution was deaerated for *ca.* 15 min before applying the voltage. The half wave potential $E_{1/2}$ was calculated approximately from $(E_{pa} + E_{pc})/2$.

In controlled potential analysis a platinum web electrode was employed as working electrode instead of glassy carbon. Counter and reference electrodes were separated from the working compartment by a glass frit and a salt bridge respectively. The electrolysis time was 40 min. The concentration of the electrolysis solution was 0.5×10^{-3} mol dm⁻³. Blank corrections were made by deducting faradaic impurity, faradaic residual and charging currents. The current–time function was integrated over the time period of the experiment (40 min).

Crystal structure determination

Data were collected on a Siemens Smart/CCD area-detector diffractometer. Data reductions and cell refinements were performed with Smart-CCD software.[22a] An absorption correction by using SADABS[22b] software was applied, which resulted in transmission coefficients ranging from 0.640 to 0.901. Structure solution and refinement were carried out on a Silicon Graphics Indy workstation using the SHELXTL program package.[23] The structure was solved by direct methods. All non-hydrogen atoms were located on the E map or successive Fourier difference syntheses. The structure was refined by full-matrix least squares techniques on F^2 with anisotropic thermal parameters for all non-hydrogen atoms. Hydrogen atoms on carbons were located geometrically and refined in riding mode, whereas those of water molecules were initially found on Fourier difference maps and then refined as restrained by using the DFIX instruction.

CCDC reference number 186/1940.

See http://www.rsc.org/suppdata/dt/a9/a909018e/ for crystallographic files in .cif format.

Other physical measurements

Elemental analyses were performed using a Perkin-Elmer 240c analytical instrument. The IR spectra were measured as a KBr disc using a Nicolet 5DX FT-IR spectrophotometer. Thermoanalysis of the complex was performed on a SDT 2960C TA thermoanalyser under an argon atmosphere with a rate of 10 °C min⁻¹. Proton NMR spectroscopy was performed on
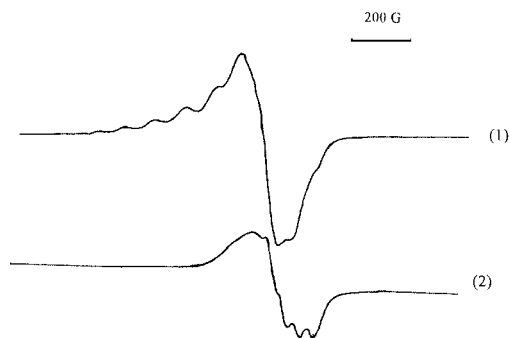
Fig. 1 The EPR spectra of the complex $[Cu_2(H_{-4}tapt)]\cdot10H_2O$ in methanol (1.0×10^{-2} mol dm^{-3}); (1) at 110 K; (2) at room temperature.

a Bruker AM-500 spectrometer. Magnetic susceptibility was measured using a CHAN-2000 Faraday-type magnetometer. X-Band EPR spectra were recorded on a Bruker ER 420 spectrometer operating at 110 K and room temperature in methanol solution with frequency modulation, 110 kHz, UV-Vis spectra by using a UV-3100 spectrometer. The electrospray mass spectrum was obtained on a Finnigan LCQ mass spectrograph, with sample concentrations of about 1.0 mmol dm^{-3}. The diluted solutions were electrosprayed at a flow rate of 5×10^{-6} dm^3 min^{-1} with a needle voltage of +4.5 kV. The temperature of the heated capillary in the interface was 200 °C and a fused silica sprayer was used. The mobile phase was an aqueous solution of methanol (1:1 v/v). The sample was run in the positive-ion mode.

Results and discussion

Characterization of the complex

The IR spectrum of ligand hydrochloride tapt·4HCl·EtOH·0.5H$_2$O shows that the C=O stretching vibration occurs at 1665 cm^{-1}. Comparing with that of $[Cu_2(H_{-4}tapt)]\cdot10H_2O$ at 1600 cm^{-1}, a shift of about 65 cm^{-1} towards lower wavenumber means the conjugation of O–C–N is strengthened after the deprotonation of the amide group. The strong and broad absorption band at 2800–3700 cm^{-1} of the complex indicates the formation of multi-hydrogen bonds involving water molecules. The molar conductivity shows that the complex is neutral, due to the deprotonation of four amide groups. Based on the above mentioned data and elemental analysis, the structure of the complex was proposed to be as in Fig. 5(a).

The complex begins to lose weight at 66 °C, and has lost 25.41% by 106 °C, corresponding to ten water molecules (calc. 24.55%). Crystal structure analysis shows the ten water molecules are composed of 2 co-ordinated and 8 crystal, but there is only one peak in the DTA curve. This is quite different from its analogue $[Cu_2(H_{-4}taet)]\cdot10H_2O$,[11] which has three weight loss processes from 40 to 128 °C. This may be due to the weak bonding of the ten water molecules in this complex. The complex begins to decompose after 240 °C.

The magnetic susceptibility (χ_m) of the complex was measured to be 3.63×10^{-3} cm^3 mol^{-1}, corresponding to a magnetic moment of 2.05 μ_B per copper(II), that is copper(II) has a single electron configuration (d^9).

The EPR spectra of the complex in methanol solution at room temperature and 110 K are shown in Fig. 1. The $g_\parallel$ region of Fig. 1 curve (1) displays a six-line set arising from hyperfine interaction between the odd electron and two copper nuclei ($I = 3/2$). This may involve partial overlapping of the $g_\parallel$ and $g_\perp$ regions because the interaction of two copper(II) nuclei ($I = 3/2$) may cause a seven-line set. From Fig. 1 curve (2), $g_{iso} = 2.085$ and $A_{iso} = 4.5$ mT $= 43.82 \times 10^{-4}$ cm^{-1} were obtained. Also the frozen solution spectrum (Fig. 1 curve (1)) yielded $A_\parallel = 9.5$ mT $= 92.52 \times 10^{-4}$ cm^{-1}, $g_\parallel = 2.226$ and $g_\perp = 2.014$ (calculated
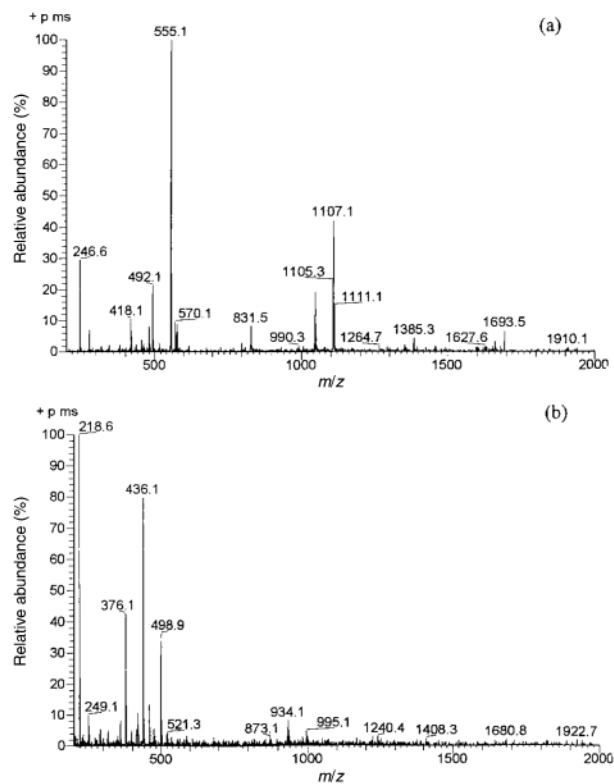
Fig. 2 The ES mass spectra of (a) $[Cu_2(H_{-4}tapt)]\cdot10H_2O$ in methanol solution and (b) $[Cu_2(H_{-4}taet)]\cdot10H_2O$ in aqueous solution.

from $g_\parallel + 2$ $g_\perp = 3$ g_{iso}). The result is similar to that for a 13-membered analogue $[Cu_2(H_{-4}bdt)]$, where bdt denotes bis(1,4,7,10-tetraazacyclotridecane-11,13-dione),[24] but is quite different from its ethyl analogue $[Cu_2(H_{-4}taet)]$ which shows no interaction between the two copper(II) nuclei in aqueous solution.[11] This may be due to the intermolecular polymerization between two molecules of $[Cu_2(H_{-4}tapt)]\cdot$ as demonstrated by electrospray mass spectra.

Electrospray mass spectra

Electrospray mass spectrometry (ES-MS) is a new technique for the characterization of unstable species and intermediates in solution since it allows preexisting ions to be transferred to the gas phase with minimum fragmentation.[25] The ES mass spectra of $[Cu_2(H_{-4}tapt)]\cdot10H_2O$ in methanol and $[Cu_2(H_{-4}taet)]\cdot10H_2O$ in aqueous solution are shown in Fig. 2 (a) and (b). In Fig. 2(a) the peak at m/z 555.1 is dominant and is assigned as $[Cu_2(H_{-4}tapt) + H^+]^+$. This may lose a Cu^{2+} ion and be further protonated. It should be noted that a dimer $[(Cu_2(H_{-4}tapt))_2 + H^+]^+$ at m/z 1107.1 with a relatively high abundance up to 42% and a trimer $[(Cu_2(H_{-4}tapt))_3 + 2H^+]^+$ at m/z 831.5 formed through self-polymerization of the species $[Cu_2(H_{-4}tapt)]$ are observed. For $[Cu_2(H_{-4}taet)]\cdot10H_2O$ in aqueous solution the situation is quite different. From Fig. 2(b) and Table 1 we can see that the abundance of the dimer $[(Cu_2(H_{-4}taet))_2 + H^+]^+$ is negligible, that is to say the monomer is dominant in the aqueous solution of $[Cu_2(H_{-4}taet)]\cdot10H_2O$ as well as in its methanol solution. In order to demonstrate the peak assignment is right, the isotopic distributions of the peak at m/z 1107, including the relative abundance and the position, were calculated by permutation and combination of ^{65}Cu, ^{63}Cu, ^{12}C and ^{13}C.[26] The calculated and observed results shown in Table 2 are in good agreement. This result further supports that the dimer is formed through intermolecular interactions. The intermolecular interaction of two copper(II) nuclei may cause a seven-line set in EPR spectra, and has been observed in many square planar macrocyclic binuclear copper(II) complexes.[27]

Table 1 Peak assignment of the complexes in Fig. 2

[Cu₂(H₋₄tapt)]·10H₂O		[Cu₂(H₋₄taet)]·10H₂O	
Peak (m/z)	Species	Peak (m/z)	Species
246.6(30)	$[Cu_2(H_{-4}tapt) - Cu^{2+} + 4H^+]^{2+}$	218.6(100)	$[Cu_2(H_{-4}taet) - Cu^{2+} + 4H^+]^{2+}$
277.1(7)	$[Cu_2(H_{-4}tapt) + 2H^+]^{2+}$	249.1(10)	$[Cu_2(H_{-4}taet) + 2H^+]^{2+}$
492.1(22)	$[Cu_2(H_{-4}tapt) - Cu^{2+} + 3H^+]^+$	376.1(43)	$[Cu_2(H_{-4}tapt) - 2Cu^{2+} + 5H^+]^+$
523.3(4)	$[(Cu_2(H_{-4}tapt))_2 - Cu^{2+} + 4H^+]^{2+}$	436.1(80)	$[Cu_2(H_{-4}taet) - Cu^{2+} + 3H^+]^+$
555.1(100)	$[Cu_2(H_{-4}tapt) + H^+]^+$	498.9(36)	$[Cu_2(H_{-4}taet) + H^+]^+$
570.1(10)	$[(Cu_2(H_{-4}tapt))_2 + CH_3OH + 2H^+]^{2+}$	934.1(8)	$[(Cu_2(H_{-4}taet))_2 - Cu^{2+} + 3H^+]^+$
831.5(8)	$[(Cu_2(H_{-4}tapt))_3 + 2H^+]^{2+}$	995.1(4)	$[(Cu_2(H_{-4}taet))_2 + H^+]^+$
1046.1(20)	$[(Cu_2(H_{-4}tapt))_2 - Cu^{2+} + 3H^+]^+$		
1107.1(42)	$[(Cu_2(H_{-4}tapt))_2 + H^+]^+$		

Note: the relative abundance is given in parentheses.

Table 2 The isotopic distribution of the $[(Cu_2(H_{-4}tapt))_2 + H^+]^+$ fragment at m/z 1107.1

Peak position		Relative abundance (%)	
Calculated	Observed	Calculated	Observed
1105.6	1105.3	53	54
1106.6	1106.2	21	38
1107.6	1107.1	100	100
1108.6	1108.1	37	42
1109.6	1109.1	72	72
1110.6	1110.1	27	31
1111.6	1111.1	24	34
1112.6	1112.0	8	6
1113.6	1113.2	4	4
1114.6	1114.3	1	2

Table 3 Equilibrium constants at 25 ± 0.01 °C, $I = 0.10$ mol dm⁻³ (KNO₃)

Reaction	$\log K^a$
$tapt + H^+ \rightleftharpoons [Htapt]^+$	9.48 ± 0.03
$[Htapt]^+ + H^+ \rightleftharpoons [H_2tapt]^{2+}$	9.15 ± 0.02
$[H_2tapt]^{2+} + H^+ \rightleftharpoons [H_3tapt]^{3+}$	8.45 ± 0.01
$[H_3tapt]^{3+} + H^+ \rightleftharpoons [H_4tapt]^{4+}$	7.67 ± 0.04
$Cu^{2+} + tapt + H^+ \rightleftharpoons [Cu(Htapt)]^{3+}$	20.00 ± 0.02
$Cu^{2+} + tapt \rightleftharpoons [Cu(tapt)]^{2+}$	13.62 ± 0.04
$Cu^{2+} + tapt \rightleftharpoons [Cu(H_{-1}tapt)]^+ + H^+$	4.78 ± 0.02
$Cu^{2+} + tapt \rightleftharpoons [Cu(H_{-2}tapt)] + 2H^+$	-4.70 ± 0.03
$2Cu^{2+} + tapt \rightleftharpoons [Cu_2tapt]^{4+}$	16.78 ± 0.02
$2Cu^{2+} + tapt \rightleftharpoons [Cu_2(H_{-2}tapt)]^{2+} + 2H^+$	4.61 ± 0.01
$2Cu^{2+} + tapt \rightleftharpoons [Cu_2(H_{-4}tapt)] + 4H^+$	-9.66 ± 0.03

[a] The equilibrium constants were also checked by the program BEST.[21b] The errors are in the range of 5%.
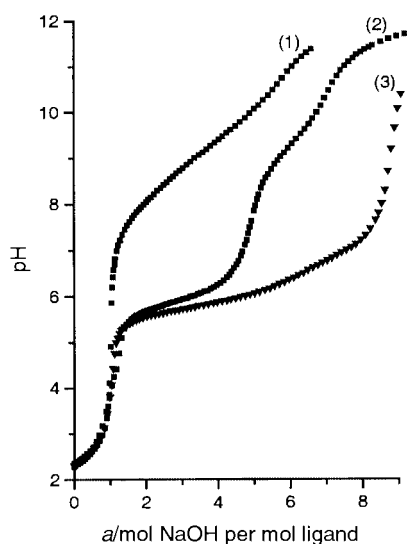
Fig. 3 pH Titration curves, $I = 0.10$ mol dm⁻³ (KNO₃), 25 °C, of (1) [tapt·4HCl] = [HNO₃] = 0.001929 mol dm⁻³, (2) [tapt·4HCl] = [Cu²⁺] = [HNO₃] = 0.002912 mol dm⁻³ and (3) [tapt·4HCl] = [HNO₃] = 0.002755, [Cu²⁺] = 0.005341 mol dm⁻³.

pH Titration

The co-ordinating ability of the ligand toward Cu²⁺ in aqueous solution has been studied by means of pH titration of a solution containing tapt·4HCl, Cu(NO₃)₂ and HNO₃ in a molar ratio of 1:1:1 or 1:2:1. Fig. 3 show the titration curves of the ligand(1) and of ligand plus Cu²⁺ with molar ratios of Cu²⁺:tapt of 1:1(2) and 2:1(3) respectively. The first inflexions of the three curves are all at about $a = 1$ (a denotes the number of moles of NaOH added per mol ligand), showing the existence of 1 mol free acid in the solutions. The titration curve (2) has two inflexions at about $a = 5$ and 7 after a short buffer region ($a = 2$–4), indicating the formation of species

[Cu(tapt)]²⁺ and [Cu(H₋₂tapt)]. The best fitting of the titration curve was obtained assuming the formation of species [Cu(Htapt)]³⁺, [Cu(tapt)]²⁺, [Cu(H₋₁tapt)]⁺, and [Cu(H₋₂tapt)]. The titration curve (3) has a long buffer region ($a = 2$–8), and the pH increases abruptly at about $a = 9$, indicating the formation of species [Cu₂(H₋₄tapt)] which gradually becomes predominant with increasing pH. Assuming [Cu₂(tapt)]⁴⁺, [Cu₂(H₋₂tapt)]²⁺, and [Cu₂(H₋₄tapt)] are formed, the best curve fitting was obtained. The values of log K are listed in Table 3. Comparing the equilibrium constants of [Cu₂-(H₋₄tapt)] with those of its ethyl analogue [Cu₂(H₋₄taet)] [Table 2 in ref. 11(b)], we may see that the electron repelling effect caused by methyl groups may improve the stability of this complex.
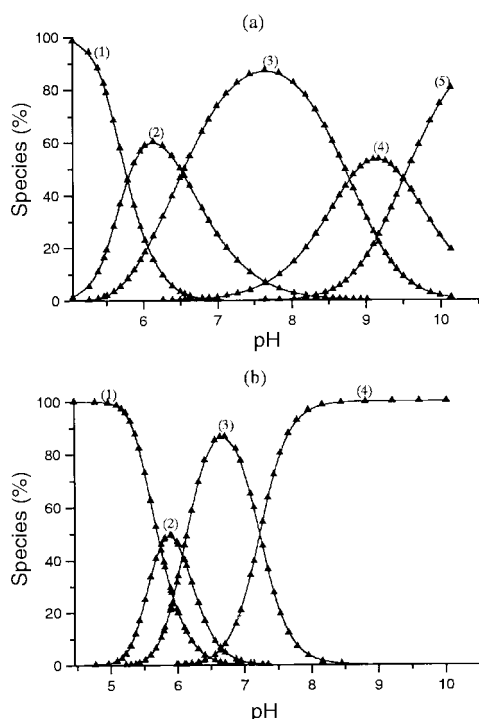
The distribution curves are shown in Fig. 4(a) and (b). In Fig. 4(b) only [Cu₂(H₋₄tapt)] exists at pH > 8.0, and at physiological pH (7.4), although [Cu₂(H₋₄tapt)] coexists with [Cu₂(H₋₂-tapt)]²⁺, the former still predominates absolutely. It is remarkable that the percentage of free Cu²⁺ is less than 0.01% at pH 7.4. Comparing with its ethyl analogue [Cu₂(H₋₄taet)],[11b] in its solution the amount of free Cu²⁺ ion is 0.07% at pH 8.3. This means that the complex has higher stability than its ethyl analogue.

Crystal structure of the complex [Cu₂(H₋₄tapt)]·10H₂O

Details of the crystal data, intensity collection and refinement are listed in Table 4. An ORTEP[28] view of the complex is shown in Fig. 5(b). Selected bond distances and angles are given in Table 5. Each copper atom has a N₄O donor set, with two nitrogen atoms of the amido groups and two nitrogen atoms of amino groups co-ordinated. The distances between amido nitrogen atoms (N(1), N(3)) and Cu^{II} (about 1.94 Å) are shorter than those between amino nitrogens (N(2), N(4)) (about

Table 4 Crystal data of complex [Cu₂(H₋₄tapt)]·10H₂O

Empirical formula	$C_{18}H_{54}Cu_2N_8O_{14}$
Formula weight	733.77
Crystal system	Triclinic
Space group	$P\bar{1}$
$a/\text{Å}$	8.4837(2)
$b/\text{Å}$	8.7611(3)
$c/\text{Å}$	11.12710(10)
$\alpha/°$	86.308(2)
$\beta/°$	86.622(2)
$\gamma/°$	78.476(2)
$U/\text{Å}^3$, Z	807.79(3), 1
T/K	293(2)
$\mu(\text{Mo-K}\alpha)/\text{mm}^{-1}$	1.388
Reflections collected	4045
Independent reflections	2733 ($R_{int} = 0.0211$)
Final $R1$, $wR2$ [$I > 2\sigma$]	0.0475, 0.1117
(all data)	0.0567, 0.1172

Table 5 Selected bond lengths (Å) and angles (°) for the complex [Cu₂(H₋₄tapt)]·10H₂O

Cu–N(1)	1.936(3)	Cu–N(3)	1.950(3)
Cu–N(4)	1.996(3)	Cu–N(2)	2.029(4)
Cu–O(3)	2.564(4)	Cu···Cu(#)	6.9798(9)
O(1)–C(1)	1.261(4)	O(2)–C(5)	1.269(4)
N(1)–C(1)	1.311(5)	N(1)–C(2)	1.462(5)
N(2)–C(3)	1.367(7)	N(3)–C(5)	1.308(5)
N(3)–C(6)	1.463(5)	N(4)–C(7)	1.452(6)
C–C(1)	1.529(5)	C–C(5)	1.531(5)
C–C(#)	1.563(7)	C(2)–C(3)	1.458(7)
C(3)–C(4)	1.515(7)	C(6)–C(7)	1.508(6)
C(7)–C(8)	1.528(6)		
N(1)–Cu–N(3)	95.74(12)	N(1)–Cu–N(4)	169.6(2)
N(3)–Cu–N(4)	84.13(13)	N(1)–Cu–N(2)	83.42(13)
N(3)–Cu–N(2)	169.0(2)	N(4)–Cu–N(2)	94.72(14)
N(1)–Cu–O(3)	103.34(13)	N(3)–Cu–O(3)	97.36(13)
N(4)–Cu–O(3)	86.99(14)	N(2)–Cu–O(3)	93.5(2)
C(1)–N(1)–C(2)	116.8(3)	C(1)–N(1)–Cu	126.7(3)
C(2)–N(1)–Cu	114.0(2)	C(3)–N(2)–Cu	110.0(3)
C(5)–N(3)–C(6)	117.5(3)	C(5)–N(3)–Cu	125.7(3)
C(6)–N(3)–Cu	113.7(2)	C(7)–N(4)–Cu	108.5(3)
C(1)–C–C(5)	118.1(3)	C(1)–C–C(#)	109.3(4)
C(5)–C–C(#)	109.0(4)	O(1)–C(1)–N(1)	124.1(3)
O(1)–C(1)–C	117.5(3)	N(1)–C(1)–C	118.2(3)
C(3)–C(2)–N(1)	110.1(4)	N(2)–C(3)–C(4)	119.1(5)
N(2)–C(3)–C(2)	116.0(5)	C(2)–C(3)–C(4)	114.9(5)
O(2)–C(5)–N(3)	125.1(3)	O(2)–C(5)–C	116.6(3)
N(3)–C(5)–C	118.2(3)	N(3)–C(6)–C(7)	108.1(3)
N(4)–C(7)–C(6)	109.8(4)	N(4)–C(7)–C(8)	113.6(4)
C(6)–C(7)–C(8)	112.9(4)		

Fig. 4 Species distribution curves (a) for curve (2) in Fig. 3, (b) for curve (3) in Fig. 3. Species: (a) (1) Cu²⁺; (2) [Cu(Htapt)]³⁺; (3) [Cu(tapt)]²⁺; (4) [Cu(H₋₁tapt)]⁺; (5) [Cu(H₋₂tapt)]; (b) (1) Cu²⁺; (2) [Cu₂(tapt)]⁴⁺; (3) [Cu₂(H₋₂tapt)]²⁺; (4) [Cu₂(H₋₄tapt)].

2.01 Å). This means the amido nitrogen atoms have stronger co-ordinating ability. A slightly distorted square-pyramidal configuration around the copper atom is completed by the additional binding of one H₂O molecule in axial position. This structure has some similarities to that of CuZnSOD. The Cu–O distance is about 2.6 Å which is longer than that of [Cu₂(H₋₄-taet)]·10H₂O (2.56 Å),[11] but shorter than that of CuZnSOD (2.8 Å).[29] The longer the Cu–O is the easier the water molecule is detached from copper in solution; the vacant co-ordination site can be occupied by ˙O₂⁻, thus the long Cu–O distance is beneficial to dismutation of ˙O₂⁻. The Cu–N distances fall in the range 1.94–2.03 Å, which are close to that of CuZnSOD (2.06 Å). The copper ion deviates by about 0.2 Å from the least-squares plane defined by N(1), N(2), N(3) and N(4) toward the H₂O molecule; this value is also close to that of CuZnSOD (0.3 Å). The two co-ordination planes are parallel with a distance of 1.60 Å. The intramolecular Cu···Cu distance is 6.9798 Å. The intermolecular Cu···Cu distance is 5.9655 Å. The angles N–Cu–N in the complex are somewhat different from those in CuZnSOD. In the complex N(2)–Cu–N(3) 169.0, N(1)–Cu–

Fig. 5 (a) Chemical structure of the complex [Cu₂(H₋₄tapt)]·10H₂O. (b) An ORTEP view.

N(4) 169.6°, but in CuZnSOD N_{His-60}–Cu–$N_{His-120}$ 157, N_{His-46}–Cu–N_{His-48} 140°.[29]

In addition to the axial water molecule, each copper center forms adducts with four water molecules. These ten water molecules in the complex form twelve intra- or inter-molecular hydrogen bonds with oxygen atoms of amido groups and hydrogen atoms of amino groups respectively. The large network of hydrogen bonds helps to stabilize the crystal. The bond distances and angles are listed in Table 6.

Table 6 Selected bond lengths (Å) and angles (°) of hydrogen bonds for the complex $[Cu_2(H_{-4}tapt)]\cdot10H_2O$

Hydrogen bond	D–H	D···A	D–H···A
O(3)–H(3D)···O(4)	0.83	2.796(6)	158
O(3)–H(3C)···O(7A)	0.84	2.773(5)	156
O(4)–H(4G)···O(5)	0.83	2.755(6)	169
O(4)–H(4F)···O(6)	0.83	2.779(5)	159
O(5)–H(5B)···O(2)	0.84	2.714(4)	162
O(5)–H(5A)···O(3A)	0.86	2.778(5)	173
O(6)–H(6C)···O(2)	0.84	2.743(4)	171
O(6)–H(6D)···O(7)	0.82	2.913(5)	165
O(7)–H(7B)···O(1)	0.83	2.731(4)	172
O(7)–H(7C)···O(1)	0.85	2.785(4)	171
N(4)–H(4E)···O(2)	0.90	3.159(5)	158
N(4)–H(4A)···O(4)	0.90	3.132(5)	154

Fig. 7 Typical kinetic plot describing the decay of absorbance of $^{\bullet}O_2^-$ at 250 nm in an O_2-saturated solution containing 1.32×10^{-5} mol dm^{-3} Cu(ClO$_4$)$_2$, 9.12×10^{-6} mol dm^{-3} ligand and 0.10 mol dm^{-3} sodium formate at pH 7.4. Inset: plot of $\ln[^{\bullet}O_2^-]_0 - \ln[^{\bullet}O_2^-]_t$ vs. t. The broken line denotes the experimental data (355 points were recorded) and the smooth curve denotes the fitted line.

$$E_{1/2} = E_p + (E_{pul}/2) \qquad (3)$$

Considering the redox potential of $^{\bullet}O_2^-$ in neutral solution,[33] we think that the Cu^{II} in the complex is able to be reduced but not oxidized by $^{\bullet}O_2^-$. This gives a clue to the mechanism of catalytical dismutation of $^{\bullet}O_2^-$ by the complex in the pulse radiolysis study.

Pulse radiolysis

When O_2-saturated solutions containing formate are radiolysed, the following species are primarily formed: $H_2O \longrightarrow {}^{\bullet}OH$, $^{\bullet}H$, H_2, $^{\bullet}e_{aq}^-$, H_2O_2, H_3O^+. At sufficiently high concentration, the formate anion transforms these free radicals into $^{\bullet}O_2^-$ within the period of the pulse. It is necessary to ensure the absence of trace metal ions, because they would make a contribution to $^{\bullet}O_2^-$ dismutation and lead to incorrect results. A blank solution at pH 7 was radiolyzed and the second-order rate constant for dismutation of $^{\bullet}O_2^-$ $k_s = 3.9 \times 10^5$ dm^3 mol^{-1} s^{-1} (pH 7.0) was obtained. The result is in agreement with that reported by Bielski and Allen[34] ($k_s = 4.0 \times 10^5$ dm^3 mol^{-1} s^{-1}, pH 7.0). Therefore it is confirmed that the impurities existing in the tested solution can be ignored.

Fig. 7 shows the decay curve of $^{\bullet}O_2^-$ vs. time t in the presence of complex recorded at 250 nm. Plotting $\ln[^{\bullet}O_2^-]_0 - \ln[^{\bullet}O_2^-]_t$ vs. time t, where $[^{\bullet}O_2^-]_0$ and $[^{\bullet}O_2^-]_t$ denote the concentration of $^{\bullet}O_2^-$ at initial stage and time t respectively, gives a straight line (Fig. 7 inset) which indicates that in the presence of the complex the decay of $^{\bullet}O_2^-$ followed pseudo-first-order kinetics, eqn. (4) where k_{obs} represents the pseudo-first-order rate

$$-d[^{\bullet}O_2^-]/dt = k_{obs}[^{\bullet}O_2^-] \qquad (4)$$

constant which can be obtained from fitting the decay curve of the concentration of $^{\bullet}O_2^-$. Integrating eqn. (4) and fitting the $^{\bullet}O_2^-$ decay curve, the square sum of error U in eqn. (5) was

$$U = \Sigma([^{\bullet}O_2^-]_i^{calc} - [^{\bullet}O_2^-]_i^{expt})^2 \qquad (5)$$

obtained: where i denotes the number of experimental points, $[^{\bullet}O_2^-]_i^{calc}$ and $[^{\bullet}O_2^-]_i^{expt}$ the calculated and experimental values for the concentration of $^{\bullet}O_2^-$ respectively. Fitting a total of 355 data points, we obtained $k_{obs} = 1006$ s^{-1} at the initial concentration of complex $[Cu_2^{II}(H_{-4}tapt)]_0 = 6.6 \times 10^{-6}$ mol dm^{-3} (pH 7.4) with log $U = -11.09$.

The catalytic mechanism of CuZnSOD and some low molecular weight mimics has been shown to involve alternate

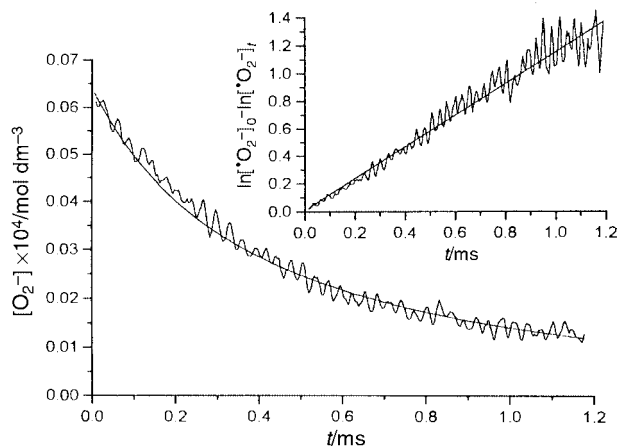

Fig. 6 Differential-pulse voltammetry profile of a solution containing 1×10^{-3} mol dm^{-3} complex (initial $E = 0.2$ V, final $E = -0.6$ V, increment in $E = 0.04$ V, amplitude = 0.05 V, pulse width = 0.06 s, sample width = 0.02 s, pulse period = 0.2 s).

Electrochemical properties of the dicopper(II) complex

During scanning from 0 to +1.0 V, the CV diagram of $[Cu_2(H_{-4}tapt)]$ displays one pair of peaks, the ratio of anodic and cathodic peak currents i_{pa}/i_{pc} being close to unity. In the same range of potential scan rates (v), the $i_p:v^{1/2}$ ratio is kept constant. The peak separation between the anodic and cathodic peaks ΔE at the scan rate 50 mV s^{-1} is 30 mV and increases with increasing scan rate (119 mV at 300 mV s^{-1}). These features are indicative of a quasi-reversible Cu^{II}Cu^{II}–Cu^{III}Cu^{III} redox process.

An electron transfer number $n = 2.27$ is obtained by controlled potential electrolysis at +0.9 V. It shows that two electrons per molecule were transferred corresponding to the production of a Cu^{III}Cu^{III} species during the positive scan and of a Cu^{II}Cu^{II} species in the reverse scan. The difference between the cathodic half-peak potential and cathodic peak potential $E_{p/2} - E_{pc}$ is about 65 mV corresponding to the separation of two redox peak $E_2° - E_1°$ (about 38 mV).[30] This also shows that the wave is due to the sequential transfer of two electrons in which the potential for the addition of the second electron is about 38 mV more negative than the first. The half-wave potential $E_{1/2}$ was calculated approximately to be +0.684 ± 0.005 V (SCE) or 0.926 V (NHE) at 50 mV s^{-1}.

During scanning from 0 to −0.75 V the CV diagram of the complex shows another pair of broad peaks. Differential-pulse voltammetry was used to determine its $E_{1/2}$ value. From the differential-pulse voltammogram (Fig. 6) we obtained $E_p = -0.088$ V, and proved that the electrode process was also a sequential two-electron-transfer quasi-reversible process Cu^{II}-Cu^{II}–Cu^{I}Cu^{I},[31] and that the two copper centers have close redox potentials. The $E_{1/2}$ value was calculated approximately by using eqn. (3),[32] where $E_{pul}/2$ denotes the pulse amplitude (50 mV), and the $E_{1/2}$ value is −0.063 V (SCE) or 0.179 V (NHE).

Table 7 The rate constants of $^\bullet O_2^-$ dismutation catalysed by mimics of CuZnSOD and their equilibrium constants in aqueous solution

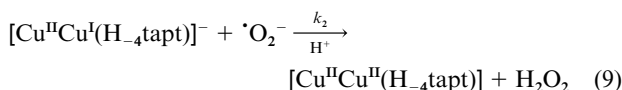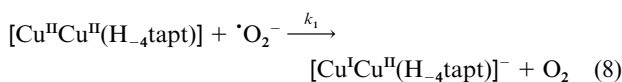|	Complex[a]	pH	k_{cat}/dm³ mol⁻¹ s⁻¹	log K[b]	Reference
1	[Cu₂(H₋₄tapt)]	7.4	1.9×10^8	-9.66	
2	[Cu₂(H₋₄taet)]	7.8	2.8×10^8	-15.22	[11(b)]
		8.3	1.6×10^8		
3	[Cu(H₋₄bdt)]	7.8	4.7×10^6	-7.09	35(a)
4	[Cu(H₋₂dt)]	7.0	7.15×10^6	-2.22	35(b)
5	[Cu(H₋₂npt)]	7.8	1.2×10^6	-2.96	37(b)
		7.0	1.9×10^6		
6	CuZnSOD	4.8–9.0	2.4×10^9		36

[a] dt denotes 1,4,7,10-tetraazacyclotridecane-11,13-dione, npt 12-(4-nitrobenzyl)-1,4,7,10-tetraazacyclotridecane-11,13-dione. [b] $nCu^{2+} + L \rightleftharpoons$ [Cu$_n$(H$_{-2n}$L)] + 2nH⁺ (L denotes ligand, n = 1 or 2); K = [Cu$_n$(H$_{-2n}$L)][H]²^n/([Cu]^n[L]).

reduction and reoxidation copper(II), eqns. (6) and (7). In

$$Cu^{II} + {}^\bullet O_2^- \longrightarrow Cu^I + O_2 \qquad (6)$$

$$Cu^I + {}^\bullet O_2^- \xrightarrow{2H^+} Cu^{II} + H_2O_2 \qquad (7)$$
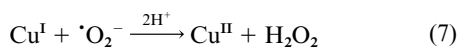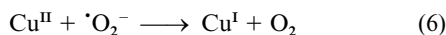
radiolysis experiments the initial concentrations of complex were 3.21×10^{-6}–1.32×10^{-5} mol dm⁻³ and that of $^\bullet O_2^-$ was 7.2×10^{-5} mol dm⁻³. The reaction kinetics of $^\bullet O_2^-$ dismutation was investigated at $[Cu_2^{II}(H_{-4}tapt)]_0 < [^\bullet O_2^-]_0$. Under an excess of $^\bullet O_2^-$, the complex catalysed dismutation of $^\bullet O_2^-$ and did not oxidize $^\bullet O_2^-$.[33] The mechanism can be described as in eqns. (8) and (9). Assuming a steady state for either $[Cu^{II}Cu^{II}$-

$$[Cu^{II}Cu^{II}(H_{-4}tapt)] + {}^\bullet O_2^- \xrightarrow{k_1}$$
$$[Cu^ICu^{II}(H_{-4}tapt)]^- + O_2 \qquad (8)$$

$$[Cu^{II}Cu^I(H_{-4}tapt)]^- + {}^\bullet O_2^- \xrightarrow[H^+]{k_2}$$
$$[Cu^{II}Cu^{II}(H_{-4}tapt)] + H_2O_2 \qquad (9)$$

(H₋₄tapt)] or [Cu^{II}Cu^I(H₋₄tapt)]⁻ respectively, the initial concentration of complex $[Cu_2^{II}(H_{-4}tapt)]_0 = [Cu^{II}Cu^I(H_{-4}tapt)^-]$ + $[Cu^{II}Cu^{II}(H_{-4}tapt)]$ and eqns. (10) and (11) are applicable. The

$$-d[^\bullet O_2^-]/dt = (2k_1k_2/(k_1 + k_2))[Cu_2^{II}(H_{-4}tapt)]_0[^\bullet O_2^-] =$$
$$k_{cat}[Cu_2^{II}(H_{-4}tapt)]_0[^\bullet O_2^-] \qquad (10)$$

$$k_{obs} = k_{cat}[Cu_2^{II}(H_{-4}tapt)]_0 \qquad (11)$$

rate constant of catalytic dismutation k_{cat} was determined by plotting k_{obs} as a function of $[Cu_2^{II}(H_{-4}tapt)]_0$ (Fig. 8). A straight line obtained goes through the origin with $R = 0.993$. So the mechanism is consistent with the experimental results. The rate constant together with results for some mimics and CuZnSOD are listed in Table 7 for comparison.

Although the activity of CuZnSOD and its analogs can be assayed by many indirect methods, these methods cannot provide absolute rate data. Pulse radiolysis is the best method to study the reaction of $^\bullet O_2^-$ dismutation in the absence of extraneous and interfering molecules.[11b,35,38] In our pulse radiolysis experiments the molar ratio of ligand and Cu(ClO₄)₂ was controlled to be 1.4:2, the excess of ligand being to ensure the concentration of free copper ion is very low. Therefore the k_{cat} value is trustworthy.

Comparing the rate constants of complex [Cu₂(H₋₄tapt)] **1** and of its ethyl analogue [Cu₂(H₋₄taet)] **2**, we can see that they are similar, but the thermodynamic stability of the former is higher than that of the latter. In Table 7 the complex **3**, [Cu₂(H₋₄bdt)] has the highest stability among the three mimics **1**, **2** and **3**, however its catalytic rate constant is about two orders of magnititude lower than that of **1** and is of the same order as those of macrocyclic complexes **4** and **5**. The backbone of the acyclic complexes is more flexible than those of **3**, **4** and **5**, and
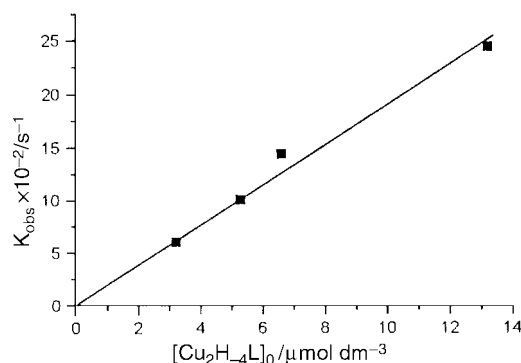
Fig. 8 Plot of pseudo-second-order rate constant of decay of $^\bullet O_2^-$ vs. the initial concentration of $[Cu^{II}_2(H_{-4}tapt)]$.

is similar to that of the protein chain of CuZnSOD, so that their configurations can be changed easily during dismutation of $^\bullet O_2^-$.[6a] Therefore they have high activity. In the complex [Cu₂(H₋₄tapt)] the introduction of a methyl group may increase the thermodynamic stability and the permeability for cells.

Acknowledgements

References

1 J. S. Valentine and D. M. Freitas, *J. Chem. Educ.*, 1985, **62**, 990.
2 (*a*) J. V. Bannister, W. H. Bannister and G. Rotilio, *CRC Crit. Rev. Biochem.*, 1987, **22**, 111; (*b*) J. K. Hurst and W. C. Barrette, *Crit. Rev. Biochem. Mol. Biol.*, 1989, **24**, 271; (*c*) J. M. McCord, *Free Radical Biol. Med.*, 1988, **4**, 9.
3 *Developments in Biochemistry*, Vol. 11 B, eds. W. H. Bannister and J. V. Bannister, Elsevier North Holland, Inc., New York, 1980.
4 J. R. J. Sorenson, *Chem. Br.*, 1984, **20**, 1110.
5 S. Kubota and J.-T. Yang, *Proc. Natl. Acad. Sci. U.SA.*, 1984, **81**, 3283; R. P. Bonomo, E. Conte, G. Impellizzeri, G. Pappalardo, R. Purrello and E. Rizzarelli, *J. Chem. Soc., Dalton Trans.*, 1996, 3093; R. N. Patel and K. B. Pandeya, *J. Inorg. Biochem.*, 1998, **72**, 109.
6 (*a*) J. Muller, K. Felix, C. Maichle, E. Lengfelder, J. Sträble and U. Weser, *Inorg. Chim. Acta*, 1995, **233**, 11; (*b*) Q.-H. Luo, Q. Lu, A.-B. Dai and L.-G. Huang, *J. Inorg. Biochem.*, 1993, **51**, 655; (*c*) J. Muller, D. Schubl, C. Maichle-Mossmer, J. Strahle and U. Weser, *J. Inorg. Biochem.*, 1999, **75**, 63; (*d*) J. Wang, Q.-H. Luo, J.-J. Zhang, M.-C. Shen, A.-D. Liu, H.-C. Gu, F.-M. Li and S.-J. Di, *Radiat. Phys. Chem.*, 1997, **49**, 527.
7 R. G. Bhirud and T. S. Srivastava, *Inorg. Chim. Acta*, 1991, **179**, 125; J. Casanova, G. Alzuet, J. Borrás and O. Carugo, *J. Chem. Soc., Dalton Trans.*, 1996, 2239; A. M. Ramadan and M. M. El-Naggar, *J. Inorg. Biochem.*, 1996, **63**, 143; R. Cao, N. Travieso, A. Fragoso, R. Villalonga, A. Diaz, M. E. Martinez, J. Alpizar and D. X. West, *J. Inorg. Biochem.*, 1997, **66**, 213.

8 (*a*) Q. Lu, Q.-H. Luo, A.-B. Dai, Z.-Y. Zhou and G.-Z. Hu, *J. Chem. Soc., Chem. Commun.*, 1990, 1429; (*b*) J. L. Pierre, P. Chautemps, S. Refaif, C. Beguin, A. E. Marzouki, G. Serratrice, E. Saint-Aman and P. Rey, *J. Am. Chem. Soc.*, 1995, **117**, 1965.

9 G. Tabbi, W. L. Driessen, J. Reedijk, R. P. Bonomo, N. Veldman and A. L. Spek, *Inorg. Chem*, 1997, **36**, 1168; P. K. Coughlin, A. E. Martin, J. C. Dewan, E. Watanabe, J. E. Bulkowski, J.-M. Lehn and S. J. Lippard, *Inorg. Chem.*, 1984, **23**, 1004; P. K. Coughlin and S. J. Lippard, *Inorg. Chem.*, 1984, **23**, 1446.

10 E. Kimura, A.Yatsunami, A. Watanabe, R. Machida, T. Koike, H. Fujioke, Y. Kuramoto, M. Sumomogi, K. Kanimitsu and A. Yamashita, *Biochim. Biophys. Acta*, 1983, **745**, 37; Z. Durackova and J. Labuda, *J. Inorg. Biochem.*, 1995, **58**, 297; E. Bienvenue, S. Choua, M.-A. Lobo-Recio, C. Marzin, P. Pacheco, P. Seta and G. Tarrag, *J. Inorg. Biochem.*, 1995, **57**, 157.

11 (*a*) S.-R. Zhu, Q.-H. Luo, M.-C. Shen, A.-B. Dai and L.-G. Huang, *Polyhedron*, 1992, **8**, 941; (*b*) C.-J. Feng, Q.-H. Luo, Z.-L. Wang, M.-C. Shen, H.-W. Wang and M.-H. Zhao, *J. Inorg. Biochem.*, 1999, **75**, 1.

12 J. A. Tainer, E. D. Getzoff, K. M. Beem, J. S. Richardson and D. C. Richardson, *J. Mol. Biol.*, 1982, **160**, 181.

13 E. Kimura, *Pure Appl. Chem.*, 1989, **61**, 823.

14 E. Kimura and R. Machida, *J. Chem. Soc., Chem. Commun.*, 1984, 499; E. Kimura, T. Koike, T. Shiota and Y. Iitaka, *Inorg. Chem.*, 1990, **29**, 4621; E. Kimura, *Pure Appl. Chem.*, 1993, **65**, 355.

15 E. Kimura, *Jpn. Kokai. Tokkyo Koho*, JP 60, 202, 869, 1984.

16 G. E. Jackson and B. S. Nakani, *J. Chem. Soc., Dalton Trans.*, 1996, 1373.

17 Y.-P. Tian, Y.-Z. Fang, Q.-H. Luo, M.-C. Shen, Q. Lu and W.-M. Shen, *Free Radical Biol. Med.*, 1992, **13**, 553.

18 L. Fabbrizzi, F. Forlini, A. Perotti and B. Seghi, *Inorg. Chem.*, 1984, **23**, 807.

19 J. E. Powell and M. A. Hiller, *J. Chem. Educ.*, 1957, **34**, 330.

20 K. N. Jha, G. L. Bolton and G. R. Freeman, *J. Phys. Chem.*, 1972, **76**, 3876.

21 (*a*) Q.-H. Luo, M.-C. Shen, Y. Ding, X.-L. Bao and A.-B. Dai, *Talanta*, 1990, **37**, 357; Q.-H. Luo, S.-R. Zhu, M.-C. Shen, S.-Y. Yu, Z. Zhang, X.-Y. Huang and Q.-J. Wu, *J. Chem. Soc., Dalton Trans.*, 1994, 1873; (*b*) A. E. Martell and R. J. Motekaitis, *The Determination and Use of Stability Constants*, 2nd Edn., VCH, New York, 1992.

22 (*a*) XSCANS (Version 2.1), Siemens Analytical X-Ray Instruments Inc., Madison, WI, 1994; (*b*) G. M. Sheldrick, Program for Empirical Absorption Correction of Area Detector Data, University of Göttingen, 1996.

23 SHELXTL (Version 5.0), Siemens Industrial Automation Inc., Analytical Instrumentation, Madison, WI, 1995.

24 A. Buttafava, L. Fabbrizzi, A. Perotti, A. Poggi and B. Seghi, *Inorg. Chem.*, 1984, **23**, 3917.

25 C. Piguel, G. Bernardinelli and G. Hopfgarter, *Chem. Rev.*, 1997, **97**, 2005.

26 J.-J. Zhang, W. Zhang, Q.-H. Luo and Y.-H. Mei, *Polyhedron*, 1999, **18**, 3637.

27 U. Casellato and P. A. Vigato, *Coord. Chem. Rev*, 1977, **23**, 31.

28 C. K. Johnson, ORTEP II, Report ORNL-5138, Oak Ridge National Laboratory, Oak Ridge, TN, 1976.

29 I. Bertini, L. Banci and M. Piccioli, *Coord. Chem. Rev.*, 1990, **100**, 67.

30 R. L. Myers and I. Shain, *Anal. Chem.*, 1969, **41**, 980.

31 R. L. Birke, M.-H. Kim and M. Strassfeld, *Anal. Chem.*, 1981, **53**, 852.

32 D. E. Richardson and H. Taube, *Inorg. Chem.*, 1981, **20**, 1278.

33 S. Goldstein, G. Czapski and D. Meyerstein, *J. Am. Chem. Soc.*, 1990, **112**, 6489; D. Klug and J. Rabani, *J. Phys. Chem.*, 1976, **80**, 587.

34 B. H. J. Bielski and A. O. Allen, *J. Phys. Chem.*, 1977, **81**, 1048.

35 (*a*) Q.-H. Luo, S.-R. Zhu, M.-C. Shen and J. Wang, *Radiat. Phys. Chem.*, 1995, **45**, 247; (*b*). Q.-H. Luo, S.-R. Zhu, M.-C. Shen, A.-B. Dai, A.-D. Liu, H.-C. Gu, F.-M. Li and S.-J. Di, *Chin. Sci. Bull.*, 1992, **14**, 1288.

36 D. Klug, J. Rabani and I. Fridovich, *J. Biol. Chem.*, 1972, **217**, 4839.

37 (*a*) G. Tabbi, T. Nauser, W. H. Koppenol and J. Reedijk, *Eur. J. Inorg. Chem.*, 1998, 1939; (*b*) Q.-H. Luo, C.-J. Feng, S.-R. Zhu, M.-C. Shen, A.-D, Lui, H.-C. Gu, F.-M. Li and S.-J. Di, *Radiat. Phys. Chem.*, 1998, **53**, 397.

38 E. Kimura, T. Koike, R. Machida, H. Nada and M. Kodama, *Inorg. Chem.*, 1984, **23**, 4181.